

# Planetary Companions around Three Intermediate-Mass G and K Giants: 18 Del, $\xi$ Aql, and HD 81688

Bun'ei SATO,<sup>1</sup> Hideyuki IZUMIURA,<sup>2,3</sup> Eri TOYOTA,<sup>4</sup> Eiji KAMBE,<sup>2</sup> Masahiro IKOMA,<sup>5</sup>  
Masashi OMIYA,<sup>6</sup> Seiji MASUDA,<sup>7</sup> Yoichi TAKEDA,<sup>8</sup> Daisuke MURATA,<sup>4</sup>

Yoichi ITOH,<sup>4</sup> Hiroyasu ANDO,<sup>8</sup> Michitoshi YOSHIDA,<sup>2</sup> Eiichiro KOKUBO,<sup>8</sup> and Shigeru IDA<sup>5</sup>

<sup>1</sup>*Global Edge Institute, Tokyo Institute of Technology, 2-12-1-S6-6 Ookayama, Meguro-ku, Tokyo  
152-8550, Japan*

*sato.b.aa@m.titech.ac.jp*

<sup>2</sup>*Okayama Astrophysical Observatory, National Astronomical Observatory, Kamogata, Okayama  
719-0232, Japan*

*izumiura@oao.nao.ac.jp, kambe@oao.nao.ac.jp, yoshida@oao.nao.ac.jp*

<sup>3</sup>*The Graduate University for Advanced Studies, Shonan Village, Hayama, Kanagawa 240-0193,  
Japan*

<sup>4</sup>*Graduate School of Science, Kobe University, 1-1 Rokkodai, Nada, Kobe 657-8501, Japan*

*toyota@kobe-u.ac.jp, yitoh@kobe-u.ac.jp, daisuke@harbor.scitec.kobe-u.ac.jp*

<sup>5</sup>*Department of Earth and Planetary Sciences, Tokyo Institute of Technology, 2-12-1 Ookayama,  
Meguro-ku, Tokyo 152-8551, Japan*

*mikoma@geo.titech.ac.jp, ida@geo.titech.ac.jp*

<sup>6</sup>*Department of Physics, Tokai University, 1117 Kitakaname, Hiratsuka, Kanagawa 259-1292, Japan*

*ohmiya@peacock.rh.u-tokai.ac.jp*

<sup>7</sup>*Tokushima Science Museum, Asutamu Land Tokushima, 45-22 Kibigadani, Nato, Itano-cho,*

*Itano-gun, Tokushima 779-0111, Japan*

*masuda@asutamu.jp*

<sup>8</sup>*National Astronomical Observatory, 2-21-1 Osawa, Mitaka, Tokyo 181-8588, Japan*

*takedayi@cc.nao.ac.jp, ando@optik.mtk.nao.ac.jp, kokubo@nao.ac.jp*

(Received 2007 October 2; accepted 2008 January 23)

## Abstract

We report the detection of 3 new extrasolar planets from the precise Doppler survey of G and K giants at Okayama Astrophysical Observatory. The host stars, namely, 18 Del (G6 III),  $\xi$  Aql (K0 III) and HD 81688 (K0 III–IV), are located at the clump region on the HR diagram with estimated masses of  $2.1 - 2.3M_{\odot}$ . 18 Del b has a minimum mass of  $10.3M_J$  and resides in a nearly circular orbit with period of 993 days, which is the longest one ever discovered around evolved stars.  $\xi$  Aql b and HD 81688 b have minimum masses of 2.8 and  $2.7 M_J$ , and reside in

nearly circular orbits with periods of 137 and 184 days, respectively, which are the shortest ones among planets around evolved stars. All of the substellar companions ever discovered around possible intermediate-mass ( $1.7 - 3.9M_{\odot}$ ) clump giants have semimajor axes larger than 0.68 AU, suggesting the lack of short-period planets. Our numerical calculations suggest that Jupiter-mass planets within about 0.5 AU (even up to 1 AU depending on the metallicity and adopted models) around  $2-3M_{\odot}$  stars could be engulfed by the central stars at the tip of RGB due to tidal torque from the central stars. Assuming that most of the clump giants are post-RGB stars, we can not distinguish whether the lack of short-period planets is primordial or due to engulfment by central stars. Deriving reliable mass and evolutionary status for evolved stars is highly required for further investigation of formation and evolution of planetary systems around intermediate-mass stars.

**Key words:** stars: individual: 18 Del — stars: individual:  $\xi$  Aql — stars: individual: HD 81688 — planetary systems — techniques: radial velocities

## 1. Introduction

Ongoing Doppler planet searches have discovered more than 200 extrasolar planets with various characteristics.<sup>1</sup> Most of them are quite different from those in our solar-system: the planets have minimum masses of  $5 M_{\oplus}$ – $15 M_J$  and are distributed in the range of orbital radii from 0.02 to 6 AU with orbital eccentricities of 0–0.9 (e.g. Butler et al. 2006). Distribution and correlation between these parameters are now used to calibrate planet formation theories by comparing with predictions from numerical simulations taking account of key processes of planet formation such as migration, disk lifetime, and variation of disk mass (Ida & Lin 2004; Alibert et al. 2005).

Properties of host stars also play an important role to constrain planet formation mechanisms. For example, frequency of planets is well correlated with metallicity of the host stars: metal-rich stars tend to harbor more planets than metal-poor ones do (Fischer & Valenti 2005; Santos et al. 2005), which supports the core-accretion scenario for the mechanism of giant planet formation. The host stars' mass can be another essential parameter. Recently, Johnson et al. (2007a) showed that frequency of planets around stars with  $1.3 \leq M/M_{\odot} < 1.9$  is as high as about 9%, compared to about 4% for solar-mass ( $0.7 \leq M/M_{\odot} < 1.3$ ) stars and about 2% for low-mass ( $< 0.7M_{\odot}$ ) K–M stars. It suggests that giant planets are more abundant in more massive stars probably because of their larger surface density of dust in proto-planetary disks (Ida & Lin 2005; Laughlin et al. 2004). However, in higher-mass stars such as B–A dwarfs ( $\geq 2M_{\odot}$ ), the shorter lifetime of the disk and the paucity of solid materials close to the central

---

<sup>1</sup> See, e.g., tables at <http://www.ciw.edu/boss/planets.html>; <http://exoplanet.eu/>

star could reduce the abundance of giant planets as a whole. The frequency of planets around such massive stars has not been established yet.

Doppler planet searches around intermediate-mass ( $\geq 1.6M_{\odot}$ ) stars have gradually expanded during these five years. Since massive stars on the main-sequence (early-type stars) are unsuitable for precise radial velocity measurements due to few absorption lines in their spectra, which are often rotationally broadened, major teams have targeted cool and slowly-rotating G and K giants and subgiants, that is, massive stars in evolved stages (Setiawan et al. 2005; Sato et al. 2003, 2007; Hatzes et al. 2005; Johnson et al. 2007b; Lovis & Mayor 2007; Niedzielski et al. 2007; Liu et al. 2007). They have succeeded in discovering 12 substellar companions so far around stars with masses of  $1.6\text{--}3.9M_{\odot}$  including clump giants and subgiants, and about a half of the host stars have masses greater than  $2M_{\odot}$ . Although the number of planets is still small, the planets begin to show different properties from those around low-mass stars: high frequency of massive planets (Lovis & Mayor 2007), lack of inner planets (Johnson et al. 2007b), and low metallicity of host stars (Pasquini et al. 2007). These properties must reflect the history of formation and evolution of planetary systems, which are not necessarily the same as those for solar-type stars. Planets around low-mass ( $< 1.6M_{\odot}$ ) giants have been also discovered from precise radial velocity surveys (Frink et al. 2002; Setiawan et al. 2003; Setiawan 2003; Hatzes et al. 2003; Döllinger et al. 2007). Comparing orbital distribution of the planets with those around low-mass dwarfs can give insight into understanding of evolution of planetary systems.

In this paper, we report on the detection of 3 new extrasolar planets around intermediate-mass G and K giants (18 Del,  $\xi$  Aql, HD 81688) from the Okayama Planet Search Program (Sato et al. 2005). We also update orbital parameters of HD 104985 b, the first planet discovered around G giants from our survey (Sato et al. 2003), by using the data collected during the past six years. Based on the extended sample, we discuss orbital properties of planets around evolved stars taking account of evolution of central stars.

## 2. Observations

Since 2001, we have been conducting a precise Doppler survey of about 300 G and K giants (Sato et al. 2005) using a 1.88 m telescope, the HIgh Dispersion Echelle Spectrograph (HIDES; Izumiura 1999), and an iodine absorption cell ( $I_2$  cell; Kambe et al. 2002) at Okayama Astrophysical Observatory (OAO). For precise radial velocity measurements, we set a wavelength range to  $5000\text{--}6100\text{\AA}$ , in which many deep and sharp  $I_2$  lines exist, and a slit width to  $200\ \mu\text{m}$  ( $0.76''$ ) giving a spectral resolution ( $R = \lambda/\Delta\lambda$ ) of 67000 by about 3.3 pixels sampling. We can typically obtain a signal-to-noise ratio  $S/N \gtrsim 200\ \text{pix}^{-1}$  for a  $V \leq 6$  star with an exposure time shorter than 30 min. We have achieved a Doppler precision of about  $6\ \text{m s}^{-1}$  over a time span of 6 years using our own analysis software for modeling an  $I_2$ -superposed stellar spectrum (Sato et al. 2002, 2005).

For abundance analysis, we take a pure ( $I_2$ -free) stellar spectrum with the same wave-

length range and spectral resolution as those for radial velocity measurements. We also take a spectrum covering Ca II H K lines in order to check the chromospheric activity (not simultaneously obtained with the radial velocity data) for stars showing large radial velocity variations. In this case, we set the wavelength range to 3800–4500 Å and the slit width to 250 μm giving a wavelength resolution of 50000. We can typically obtain  $S/N \simeq 20 \text{ pix}^{-1}$  at the Ca II H K line cores for a  $B = 6$  star with a 30 min exposure. The reduction of echelle data (i.e. bias subtraction, flat-fielding, scattered-light subtraction, and spectrum extraction) is performed using the IRAF<sup>2</sup> software package in the standard way.

### 3. Stellar Properties, Radial Velocities, and Orbital Solutions

#### 3.1. 18 Del

18 Del (HR 8030, HD 199665, HIP 103527) is listed in the Hipparcos catalog (ESA 1997) as a G6 III: giant star with a  $V$  magnitude  $V = 5.51$ , a color index  $B - V = 0.934$ , and the Hipparcos parallax  $\pi = 13.68 \pm 0.70$  mas, corresponding to a distance of  $73.1 \pm 3.7$  pc and an absolute magnitude  $M_V = 1.15$  taking account of correction of interstellar extinction  $A_V = 0.04$  based on the Arenou et al’s (1992) table. *Hipparcos* made a total of 175 observations of the star, revealing a photometric stability down to  $\sigma = 0.007$  mag. Figure 1 shows a Ca II H line for the star obtained with HIDES revealing slight core reversal in the line. X-ray luminosity for the star was derived to  $L_X = 3.3 \times 10^{29} \text{ erg s}^{-1}$  from the *ROSAT* measurements (Hünsch et al. 1998), suggesting that the star is slightly chromospherically active. However, the reversal is not significant compared to those in other chromospherically active stars in our sample such as HD 120048 (Figure 1), which shows velocity scatter of about  $30 \text{ m s}^{-1}$ . Thus, although the correlation between chromospheric activity and intrinsic radial velocity “jitter” for giants have not been well established yet, the jitter of 18 Del is probably expected to be no larger than that of HD 120048. Further discussions are presented in Section 4.

The atmospheric parameters and the Fe abundance of the star were determined based on the spectroscopic approach using the equivalent widths of well-behaved Fe I and Fe II lines (cf. Takeda et al. 2002 for a detailed description of this method). We obtained  $T_{\text{eff}} = 4979$  K,  $\log g = 2.82 \text{ cm s}^{-2}$ ,  $v_t = 1.22 \text{ km s}^{-1}$ , and  $[\text{Fe}/\text{H}] = -0.05$  for the star. The bolometric correction was estimated to  $B.C. = -0.39$  based on the Kurucz (1993)’s theoretical calculation. With use of these parameters and theoretical evolutionary tracks of Lejeune & Schaerer (2001), we derived the fundamental stellar parameters,  $L = 40L_\odot$ ,  $R = 8.5R_\odot$ , and  $M = 2.3M_\odot$ , as summarized in Table 1. The procedure described here is the same as that adopted in Takeda et al. (2005) (see subsection 3.2 of Takeda et al. (2005) and Note of Table 1 for uncertainties

---

<sup>2</sup> IRAF is distributed by the National Optical Astronomy Observatories, which is operated by the Association of Universities for Research in Astronomy, Inc. under cooperative agreement with the National Science Foundation, USA.

involved in the stellar parameters). The position of the star on the HR diagram is shown in Figure 2 together with other planet-harboring stars in this paper. da Silva et al. (2006) obtained  $2.13 \pm 0.13 M_{\odot}$  for the mass of the star based on  $T_{\text{eff}} = 5089 \pm 70$  K,  $\log g = 2.93 \pm 0.08$  cm s $^{-2}$ , and  $[\text{Fe}/\text{H}] = 0.05 \pm 0.05$ . Although the  $T_{\text{eff}}$  is about 100 K higher than that we obtained, the mass for the star reasonably agrees with our estimate.

We collected a total of 51 radial velocity data of 18 Del between 2002 August and 2007 June, with a typical S/N of 200 pix $^{-1}$  for an exposure time of about 900 s. The observed radial velocities are shown in Figure 3 and are listed in Table 2 together with their estimated uncertainties, which were derived from an ensemble of velocities from each of  $\sim 200$  spectral regions (each 4–5Å long) in every exposure. The sinusoidal variability in the radial velocities is visible to the eye and it can be well fitted by a Keplerian orbit with a period  $P = 993.3 \pm 3.2$  days, a velocity semiamplitude  $K_1 = 119.4 \pm 1.3$  m s $^{-1}$ , and an eccentricity  $e = 0.08 \pm 0.01$ . The resulting model is shown in Figure 3 overplotted on the velocities, and its parameters are listed in Table 3. The uncertainty of each parameter was estimated using a Monte Carlo approach. We generated 100 fake datasets by adding random Gaussian noise corresponding to velocity measurement errors to the observed radial velocities in each set, then found the best-fit Keplerian parameters for each, and examined the distribution of each of the parameters. The rms scatter of the residuals to the Keplerian fit is 15.4 m s $^{-1}$ , which is comparable to the scatters of giants with the same  $B - V$  as 18 Del in our sample (Sato et al. 2005). Adopting a stellar mass of  $2.3 M_{\odot}$ , we obtain a minimum mass for the companion  $m_2 \sin i = 10.3 M_{\text{J}}$  and a semimajor axis  $a = 2.6$  AU. The companion has the longest orbital period ever discovered around evolved stars.

We found that the residuals showed a decreasing trend with a slope of about  $-4$  m s $^{-1}$  yr $^{-1}$ , suggesting the existence of an outer companion (Figure 4). Keplerian orbital fit including a linear trend slightly improves the quality of fit, decreasing the rms scatter from 15.4 m s $^{-1}$  to 13.6 m s $^{-1}$  and the reduced  $\chi^2$  from  $\chi^2_{\text{notrend}} = 6.3$  to  $\chi^2_{\text{trend}} = 5.0$ . To assess the significance of this trend, we evaluated a false-alarm probability ( $FAP$ ), the probability that noise mimics the observed trend, by using a bootstrap analysis which is the same as adopted in Wright et al. (2007). We scrambled the residuals in a random manner while keeping fixed the observation time, and created a mock set of radial velocities by adding the residuals back to the best-fit Keplerian radial velocity curve. We created 100 such mock data sets, and obtained  $\Delta\chi^2 = \chi^2_{\text{trend}} - \chi^2_{\text{notrend}}$  for each set. Eight of the 100 data sets showed  $\Delta\chi^2$  less than that for the original data set, which means the  $FAP$  is 8%. Considering the  $FAP$ , we can not say that the observed trend is significant at this stage.

### 3.2. $\xi$ Aql

$\xi$  Aql (HR 7595, HD 188310, HIP 97938) is a K0 III giant star with a  $V$  magnitude  $V = 4.71$ , a color index  $B - V = 1.023$ , and a trigonometric parallax  $\pi = 15.96 \pm 1.01$  mas (ESA

1997), placing the star at a distance of  $62.7 \pm 4.0$  pc. The distance and an estimated interstellar extinction  $A_V = 0.10$  (Arenou et al. 1992) yield an absolute magnitude for the star  $M_V = 0.63$ . *Hipparcos* made a total of 98 observations of the star, revealing a photometric stability down to  $\sigma = 0.004$  mag. Ca II H K lines of the star show no significant emission in the line cores as shown in the Figure 1, suggesting that the star is chromospherically inactive. The atmospheric parameters, Fe abundance, and other fundamental parameters of the star are listed in Table 1. The  $[\text{Fe}/\text{H}]$  of  $-0.21$  is consistent with the value of  $-0.15$  from Taylor (1999) within the error. Gray and Brown (2001) obtained  $T_{\text{eff}} = 4670$  K for the star based on line-depth-ratio analysis, which is  $\sim 100$  K lower than our estimate (4780 K). Uncertainties in the mass and the radius are considered to be similar to those for 18 Del (see Note of Table 1).

We collected a total of 26 radial velocity data of  $\xi$  Aql between 2004 April and 2007 June, with a typical S/N of  $200 \text{ pix}^{-1}$  for an exposure time of about 300 s. The observed radial velocities are shown in Figure 5 and are listed in Table 4 together with their estimated uncertainties. Lomb-Scargle periodogram (Scargle 1982) of the data exhibits a dominant peak at a period of 137 days. To assess the significance of this periodicity, we estimated *FAP*, using a bootstrap randomization method in which the observed radial velocities were randomly redistributed, keeping fixed the observation time. We generated  $10^5$  fake datasets in this way, and applied the same periodogram analysis to them. Only 2 fake datasets exhibited a periodogram power higher than the observed dataset. Therefore, the *FAP* is  $2 \times 10^{-5}$ . The observed radial velocities can be well fitted by a circular orbit with a period  $P = 136.75 \pm 0.25$  days and a velocity semiamplitude  $K_1 = 65.4 \pm 1.7 \text{ m s}^{-1}$ . The resulting model is shown in Figure 5, and its parameters are listed in Table 3. The uncertainty of each parameter was estimated using a Monte Carlo approach as described in Section 3.1. The rms scatter of the residuals to the Keplerian fit was  $22.3 \text{ m s}^{-1}$ , which is slightly larger than the typical scatter of giants with  $B - V \simeq 1.0$  in our sample (Sato et al. 2005). Adopting a stellar mass of  $2.2 M_\odot$ , we obtain a minimum mass for the companion of  $m_2 \sin i = 2.8 M_J$  and a semimajor axis of  $a = 0.68$  AU. The companion has the shortest orbital period ever discovered among evolved stars.

### 3.3. HD 81688

HD 81688 (HR 3743, HIP 46471) is classified in the *Hipparcos* catalog (ESA 1997) as a K0 III–IV star with a *V* magnitude  $V = 5.40$ , a color index  $B - V = 0.993$ . The *Hipparcos* parallax  $\pi = 11.33 \pm 0.84$  mas corresponds to a distance of  $88.3 \pm 6.5$  pc and yields an absolute magnitude  $M_V = 0.57$  corrected by interstellar extinction  $A_V = 0.10$  (Arenou et al. 1992). *Hipparcos* made a total of 107 observations of the star, revealing a photometric stability down to  $\sigma = 0.006$  mag. Ca II H K lines of the star show no significant emission in the line cores, suggesting that the star is chromospherically inactive (Figure 1). The atmospheric parameters, Fe abundance, and other fundamental parameters of the star are listed in Table 1. Mishenina et al. (2006) obtained  $T_{\text{eff}} = 4789$  K (from line-depth-ratio analysis),  $\log g = 2.3 \text{ cm s}^{-2}$ ,  $v_t =$

1.3 km s<sup>-1</sup>, and [Fe/H] = -0.23 for the star. While the [Fe/H] is  $\sim 0.1$  dex higher than our estimate, other parameters reasonably agree with those we obtained. Although uncertainties in the mass and the radius are considered to be similar to those for 18 Del, systematic error up to  $\sim 0.5M_{\odot}$  could exist depending on adopted stellar evolutionary models (see Note of Table 1).

We collected a total of 81 radial velocity data of HD 81688 between 2003 March and 2007 April, with a typical S/N of 200 pix<sup>-1</sup> for an exposure time of about 900 s. The observed radial velocities are shown in Figure 6 and are listed in Table 5 together with their estimated uncertainties. Lomb-Scargle periodogram (Scargle 1982) of the data exhibits a dominant peak at a period of 182 days with a  $FAP < 1 \times 10^{-5}$ , which was estimated by the same method as described in Section 3.1. The observed radial velocities can be well fitted by a circular orbit with a period  $P = 184.02 \pm 0.18$  days and a velocity semiamplitude  $K_1 = 58.58 \pm 0.97$  m s<sup>-1</sup>. The resulting model is shown in Figure 6, and its parameters are listed in Table 3. The uncertainty of each parameter was estimated using a Monte Carlo approach as described in Section 3.1. Adopting a stellar mass of  $2.1 M_{\odot}$ , we obtain a minimum mass for the companion of  $m_2 \sin i = 2.7 M_J$  and a semimajor axis of  $a = 0.81$  AU.

The residuals to the Keplerian fit exhibit non-random variations in some periods of time, which may be due to stellar activity or additional companions. We performed periodogram analysis (Scargle 1982) to the residuals and found peaks at periods around 13, 25, and 55 days. However, the  $FAP$ 's for the peaks are larger than 0.5, which is not considered to be significant at this stage (some of them may be affected by aliasing). More dense sampling of data will help discriminate if the periods are real or not.

### 3.4. HD 104985

HD 104985 (HR 4609, HIP 58952) is the first planet-harboring star discovered from our survey (Sato et al. 2003). It is classified in the Hipparcos catalog (ESA 1997) as a G9 III giant star with a  $V$  magnitude  $V = 5.78$ , a color index  $B - V = 1.029$ , and a parallax  $\pi = 9.80 \pm 0.52$  mas, corresponding to a distance of  $102.0 \pm 5.4$  pc and an absolute magnitude  $M_V = 0.74$ .

The atmospheric parameters of the star were updated by Takeda et al. (2005) from those listed in the discovery paper by Sato et al. (2003) to:  $T_{\text{eff}} = 4877$  K,  $\log g = 2.85$  (cm s<sup>-2</sup>),  $v_t = 1.31$  (km s<sup>-1</sup>), and [Fe/H] = -0.15. Based on these parameters and the bolometric correction of  $B.C. = -0.43$  (Kurucz 1993), Takeda et al. (2005) obtained the fundamental stellar parameters of  $L = 60L_{\odot}$ ,  $R = 11R_{\odot}$ , and  $M = 2.3M_{\odot}$ .<sup>3</sup>

After the discovery of the planet around HD 104985 in 2003, we have continued observations of the star and collected a total of 52 data points between 2001 March and 2007 April.

---

<sup>3</sup> Sato et al. (2003) obtained a mass for the star of  $1.6 M_{\odot}$  based on the metallicity [Fe/H] = -0.35 and evolutionary tracks from Girardi et al. (2000). The tracks tend to give  $\lesssim 0.5M_{\odot}$  lower mass compared to those from Lejeune and Schaerer (2001) for  $\lesssim 2M_{\odot}$  giants with  $Z = 0.008$  ([Fe/H] = -0.4).

The observed radial velocities are shown in Figure 7 and are listed in Table 6 together with their estimated uncertainties. Based on the extended data set, we updated the orbital parameters of the planet:  $P = 199.505 \pm 0.085$  days,  $K_1 = 166.8 \pm 1.3$  m s<sup>-1</sup>, and  $e = 0.090 \pm 0.009$ . The resulting Keplerian model is shown in Figure 6, and the parameters are listed in Table 3. Adopting a stellar mass of  $2.3M_\odot$ , we obtain a minimum mass for the companion of  $m_2 \sin i = 8.3M_J$  and a semimajor axis of  $a = 0.95$  AU. We can not find any additional periodic signals or long-term trend in their radial velocities for now.

#### 4. Line Shape Analysis

To investigate other causes producing apparent radial velocity variations such as pulsation and rotational modulation rather than orbital motion, spectral line shape analysis was performed with use of high resolution stellar templates followed by the technique of Sato et al. (2007). In our technique, we extract a high resolution iodine-free stellar template from several stellar spectra contaminated by iodine lines (Sato et al. 2002). Basic procedure of the technique is as follows; first, we model observed star+I<sub>2</sub> spectrum in a standard manner but using the initial guess of the intrinsic stellar template spectrum. Next we take the difference between the observed star+I<sub>2</sub> spectrum and the modeled one. Since the difference is mainly considered to be due to an imperfection of the initial guess of the stellar template spectrum, we revise the initial guess taking account of the difference and model the observed star+I<sub>2</sub> spectrum using the revised guess of the template. We repeat this process until we obtain sufficient agreement between observed and modeled spectrum. We take average of thus obtained stellar templates from several observed star+I<sub>2</sub> spectra to increase S/N ratio of the template. Details of this technique are described in Sato et al. (2002).

For spectral line shape analysis, we extracted two stellar templates from several star+I<sub>2</sub> spectra at the peak and valley phases of observed radial velocities for each star. Then, cross correlation profiles of the two templates were calculated for 30–50 spectral segments (4–5Å width each) in which severely blended lines or broad lines were not included. Three bisector quantities were calculated for the cross correlation profile of each segment: the velocity span (BVS), which is the velocity difference between two flux levels of the bisector; the velocity curvature (BVC), which is the difference of the velocity span of the upper half and lower half of the bisector; and the velocity displacement (BVD), which is the average of the bisector at three different flux levels. We used flux levels of 25%, 50%, and 75% of the cross correlation profile to calculate the above quantities. Resulting bisector quantities for 18 Del, ξ Aql, HD 81688, and HD 104985 are listed in Table 7. As expected from the planetary hypothesis, both of the BVS and the BVC are identical to zero, which means that the cross correlation profiles are symmetric, and the average BVD is consistent with the velocity difference between the two templates at the peak and valley phases of observed radial velocities ( $\simeq 2K_1$ ). The BVS for HD 104985 is slightly large compared to those for other stars, suggesting the higher intrinsic



variability for HD 104985. It may be consistent with the large rms scatters of the residuals to the Keplerian fit ( $\sigma = 26.6 \text{ m s}^{-1}$ ) for the star. However, the BVS value is only one thirtieth of the BVD and thus it is unlikely that the observed radial velocity variations are produced by the intrinsic activity such as pulsation or rotational modulation. Based on these results, we conclude that the radial velocity variability observed in these 4 stars are best explained by orbital motion.

## 5. Discussion

We discovered a total of 6 substellar companions around G and K giants so far from our Okayama Planet Search Program (Sato et al. 2003, 2007; Liu et al. 2007; this work). The host stars are located at the clump region on the HR diagram and their masses are estimated to 2.1–2.7  $M_{\odot}$ . When we include 6 more planets discovered around possible clump giants by other teams (Table 8), the mass of the host stars ranges from 1.7 to 3.9  $M_{\odot}$ . These discoveries definitely indicate that planets can form around intermediate-mass stars, such as B–A dwarfs, as well as around low-mass ones. The extended sample enables us to clarify the properties of the planets around intermediate-mass clump giants; the planets have minimum masses of 2.3–19.8  $M_J$ , semimajor axes of 0.68–2.6 AU, and eccentricities of 0–0.4. In Figure 8, we plotted the minimum mass against the semimajor axis. Since intrinsic variability in radial velocity of clump giants is typically 10–20  $\text{m s}^{-1}$  (Sato et al. 2005), it is normally difficult to detect planets with  $\lesssim 2M_J$  at  $\simeq 1$  AU around a  $2M_{\odot}$  star, which can produce radial velocity semiamplitude of 40  $\text{m s}^{-1}$  at most. Such lower-mass planets can be detected around stars with small intrinsic variability ( $< 10 \text{ m s}^{-1}$ ) like subgiants (Johnson et al. 2007b). While the largest semimajor axis of 2.6 AU is limited by the time baseline of the current surveys, the lack of short-period planets with  $a \lesssim 0.7$  AU appears to be real at least for relatively massive planets because stellar radius of clump giants is typically 10–20  $R_{\odot}$ , which correspond to 0.05–0.1 AU, and thus we should be able to find planets with  $0.1 \lesssim a \lesssim 0.7$  AU if they exist. In Figure 9, we plotted the eccentricity against the semimajor axis together with lines expressing different periastron distances ( $q = a(1 - e)$ ). From the view point of orbital evolution of planets, periastron distance is more essential rather than semimajor axis because tidal interaction between a planet and a central star strongly depends on distance between them. As shown in the figure, all the companions around clump giants have  $q \geq 0.68$  AU, while those around intermediate-mass subgiants (1.6–1.9  $M_{\odot}$ ) and low-mass K giants ( $< 1.6M_{\odot}$ ) have  $q \geq 0.69$  AU and  $\geq 0.33$  AU, respectively. Since a lot of planets with  $q \leq 0.3$  AU have been found around solar-type dwarfs (open circles), the lack of inner planets around low-mass K giants can be due to engulfment by the central stars.

We here examined whether the lack of short-period planets around clump giants could be reproduced by evolutionary effect of the central stars based on available stellar evolutionary models. If the clump giants are post-RGB (core helium burning) stars, short-period planets

around them might have been engulfed by the central stars at the tip of RGB due to tidal torque from the expanding stellar surface. We numerically traced tidal evolution of a planetary orbit ( $\dot{a}_{tide}$ ) based on equations from Zahn (1989) and stellar evolutionary tracks from Lejeune & Schaerer (2001) (LS01) and Claret (2004,2006,2007). We assumed a circular orbit but the result can be applied to the case of an eccentric orbit by replacing the semimajor axis with periastron distance. We also took account of orbital evolution due to mass loss as  $\dot{a}_{loss} = \dot{M}_* a / M_*$ , where  $M_*$  is a mass of the central star. Mass loss of the central star makes planets move outward because of their weakened gravitational pull on the planets (e.g., Sackmann et al. 1993; Duncan & Lissauer 1998). Thus, net change of orbital radius of a planet is expressed as  $\dot{a} = \dot{a}_{tide} + \dot{a}_{loss}$ . We finally found out, however, that orbital change due to mass loss is negligible in RGB phase for planets around 2–3  $M_\odot$  stars because the mass loss of those stars in RGB phase is negligible based on the adopted evolutionary tracks. It excludes the scenario that inner planets were pushed out to 0.7 AU resulting in the lack of planets within the radius. The mass loss may be important in the case of lower-mass stars (Silvotti et al. 2007). From the orbital calculations, we found out that Jupiter-mass planets within about 3–4  $R_*$  (radius of a central star) can be engulfed by the central stars due to the tidal torque during RGB phase. Our results predict that, around 2–3  $M_\odot$  stars, only planets within 0.2 AU are engulfed by the central stars at the bottom of RGB ( $R_* \lesssim 10R_\odot$ ), but those within about 0.5 AU can be done at the tip of RGB ( $R_* \simeq 25 - 40R_\odot$ ). The critical orbital radius at the tip of RGB for  $2M_\odot$  can be larger than 1 AU in the cases of  $Z = 0.04$  for LS01 and  $Z = 0.019$  and  $0.04$  for Claret’s tracks. When we assume that most of the clump giants are post-RGB stars, it might be natural that we could not find short-period planets around them even if they had originally existed. Typically small orbital eccentricities ( $e = 0 - 0.4$ ) of the planets discovered around clump giants compared to those around dwarfs may favor this scenario, in which the planetary orbits could be tidally circularized during RGB phase.

There can be another possibility, however, that short-period planets are primordially rare around intermediate-mass stars. Lack of short-period planets around less evolved subgiants with 1.6–1.9 $M_\odot$  (Figure 9; Johnson et al. 2007b), which are considered to be first ascent on RGB, may favor this scenario. Such dependence of orbital distribution of planets on host star’s mass is predicted by Burkert & Ida (2007). They pointed out that in observed data for F–K dwarfs, there may be a paucity of planets in  $a = 0.1 - 0.6$  AU around  $\geq 1.2M_\odot$  stars (F dwarfs) while the semimajor axis distribution is more uniform around G and K dwarfs. They showed that the gap could be produced by shorter viscous diffusion timescale of disks possibly due to smaller disk size for more massive stars, which can limit the efficiency of type II migration of giant planets and keep planets residing close to initial formation locations beyond snow lines at several AU. The lack of inner planets around subgiants with 1.6–1.9 $M_\odot$  might be consistent with this prediction. It is not clear whether this is also the case for more massive stars with  $\geq 2M_\odot$ . Around such stars, due to distant snow line ( $>10$  AU) and averagely large disk mass,

the main region for giant planet formation could be closer to the central stars compared to around low-mass stars. On the other hand, Kennedy and Kenyon (2007) recently showed that the snow line distance changes weakly with stellar mass if they take account of disk and pre-main-sequence evolution. More detailed theoretical modeling is required for planet formation around stars with  $\geq 2M_{\odot}$ .

In order to further investigate formation and evolution of planetary systems around massive stars via evolved giants, it is important to derive their accurate mass and evolutionary status. It is normally difficult, however, because stars with different mass and evolutionary status can occupy similar position in the giant branch on the HR diagram. To overcome this difficulty, asteroseismology will be a powerful tool, which can probe stellar interior by using tiny stellar oscillations. Such oscillations were actually detected in some G and K giants (e.g., Frandsen et al. 2002; Hatzes & Zechmeister 2007; Ando et al. 2007). Applying this technique to the planet-harboring evolved stars is highly encouraged.

This research is based on data collected at Okayama Astrophysical Observatory (OAO), which is operated by National Astronomical Observatory of Japan (NAOJ). We are grateful to all the staff members of OAO for their support during the observations. M.I. thanks Dr. A. Claret for his helpful comments on his evolutionary tracks. Data analysis was in part carried out on “sb” computer system operated by the Astronomical Data Analysis Center (ADAC) and Subaru Telescope of NAOJ. We thank the National Institute of Information and Communications Technology for their support on high-speed network connection for data transfer and analysis. B.S. is supported by Grant-in-Aid for Young Scientists (B) No.17740106, and H.I., H.A., and M.Y. are supported by Grant-in-Aid for Scientific Research (C) No.13640247, (B) No.17340056, (B) No.18340055, respectively, from the Japan Society for the Promotion of Science (JSPS). E.T, D.M, and Y.I. are supported by “The 21st Century COE Program: The Origin and Evolution of Planetary Systems” in Ministry of Education, Culture, Sports, Science and Technology (MEXT). E.K. and S.I. are partially supported by MEXT, Japan, the Grant-in-Aid for Scientific Research on Priority Areas, “Development of Extra-Solar Planetary Science.” This research has made use of the SIMBAD database, operated at CDS, Strasbourg, France.

## References

- Alibert, Y., Mordasini, C., Benz, W., Winisdoerffer, C. 2005, *A&A*, 434, 343  
Ando, H., Tan, K., Kambe, E., Sato, B., & Zhao, G. 2008, *PASJ*, in press  
Arenou, F., Grenon, M., & Gomez, A. 1992, *A&A*, 258, 104  
Burkert, A. & Ida, S. 2007, *ApJ*, 660, 845  
Butler, R.P. et al. 2006, *ApJ*, 646, 505  
Claret, A. 2007, *A&A*, 467, 1389

- Claret, A. 2006, *A&A*, 453, 769  
Claret, A. 2004, *A&A*, 424, 919  
da Silva, L. et al. 2006, *A&A*, 458, 609  
de Medeiros, J. R., & Mayor, M. 1999, *A&AS*, 139, 433  
Döllinger, M.P., Hatzes, A.P., Pasquini, L., Guenther, E.W., Hartmann, M., Girardi, L., & Esposito, M. 2007, *A&A*, 472, 649  
Duncan, M.J. & Lissauer, J.J. 1998, *Icarus*, 134, 303  
ESA. 1997, *The Hipparcos and Tycho Catalogues* (ESA SP-1200; Noordwijk: ESA)  
Fischer, D.A. & Valenti, J. 2005, *ApJ*, 622, 1102  
Frandsen, S. et al. 2002, *A&A*, 394, 5  
Frink, S., Mitchell, D.S., Quirrenbach, A., Fischer, D., Marcy, G.W., & Butler, R.P. 2002, *ApJ*, 576, 478  
Girardi, L., Bressan, A., Bertelli, G., & Chiosi, C. 2000, *A&AS*, 141, 371  
Gray, D.F. & Brown, K. 2001, *PASP*, 113, 723  
Hatzes, A.P. et al. 2003, *ApJ*, 599, 1383  
Hatzes, A.P., Guenther, E.W., Endl, M., Cochran, W.D., Döllinger, M.P., & Bedalov, A. 2005, *A&A*, 437, 743  
Hatzes, A.P. & Zechmeister, M. 2007, *ApJ*, 670, L37  
Hünsch, M., Schmitt, J. H. M. M., & Voges, W. 1998, *A&AS*, 127, 251  
Ida, S. & Lin, D.N.C. 2004, *ApJ*, 604, 388  
Ida, S. & Lin, D.N.C. 2005, *ApJ*, 626, 1045  
Izumiura, H. 1999, in *Proc. 4th East Asian Meeting on Astronomy*, ed. P.S. Chen (Kunming: Yunnan Observatory), 77  
Johnson, J.A., Butler, R.P., Marcy, G.W., Fischer, D.A., Vogt, S.S., Wright, J.T., & Peek, K.M.G. 2007a, *ApJ*, 670, 833  
Johnson, J.A. et al. 2007b, *ApJ*, 665, 785  
Kambe, E. et al. 2002, *PASJ*, 54, 865  
Kennedy, G.M. and Kenyon, S.J. 2007, *ApJ* in press  
Kurucz, R. L. 1993, *Kurucz CD-ROM*, No. 13 (Harvard-Smithsonian Center for Astrophysics)  
Laughlin, G., Bodenheimer, P. & Adams, F.C. 2004, *ApJ*, 612, 73  
Lejeune, T. & Schaerer, D. 2001, *A&A*, 366, 538  
Liu, Y.J. et al. 2007, *ApJ*, 672, 553  
Lovis, C. & Mayor, M. 2007, *A&A*, 472, 657  
Mishenina, T.V. et al. 2006, *A&A*, 456, 1109  
Niedzielski, A. et al. 2007, *ApJ*, 669, 1354  
Pasquini, L. et al. 2007, *A&A*, 473, 979  
Sackmann, I.J., Boothroyd, A.I., & Kraemer, K.E. 1993, *ApJ*, 418, 457  
Santos, N.C., Israelian, G., Mayor, M., Bento, J.P., Almeida, P.C., Sousa, S.G. & Ecuivillon, A. 2005, *A&A*, 437, 1127  
Sato, B. et al. 2003, *ApJ*, 597, L157  
Sato, B., Kambe, E., Takeda, Y., Izumiura, H., & Ando, H. 2002, *PASJ*, 54, 873

Sato, B., Kambe, E., Takeda, Y., Izumiura, H., Masuda, S. & Ando, H. 2005, PASJ, 57, 97  
Sato, B. et al. 2007, ApJ, 661, 527  
Scargle, J. D. 1982, ApJ, 263, 835  
Setiawan, J. et al. 2003, A&A, 398, L19  
Setiawan, J. DARWIN/TPF and the Search for Extrasolar Terrestrial Planets, 22-25 April 2003, Heidelberg, Germany. Edited by M. Fridlund, T. Henning, compiled by H. Lacoste. ESA SP-539, Noordwijk, Netherlands: ESA Publications Division, 2003, p. 595-598  
Setiawan, J. et al. 2005, A&A, 437, 31  
Silvotti, R. et al. 2007, Nature, 449, 189  
Takeda, Y., Ohkubo, M., & Sadakane, K. 2002, PASJ, 54, 451  
Takeda, Y, Sato, B., Kambe, E., Izumiura, H., Masuda, S., & Ando, H. 2005, PASJ, 57, 109  
Taylor, B.J. 1999, A&AS, 134, 523  
Wright, J.T. et al. 2007, ApJ, 657, 533  
Zahn, J.-P. 1989, A&A, 220, 112

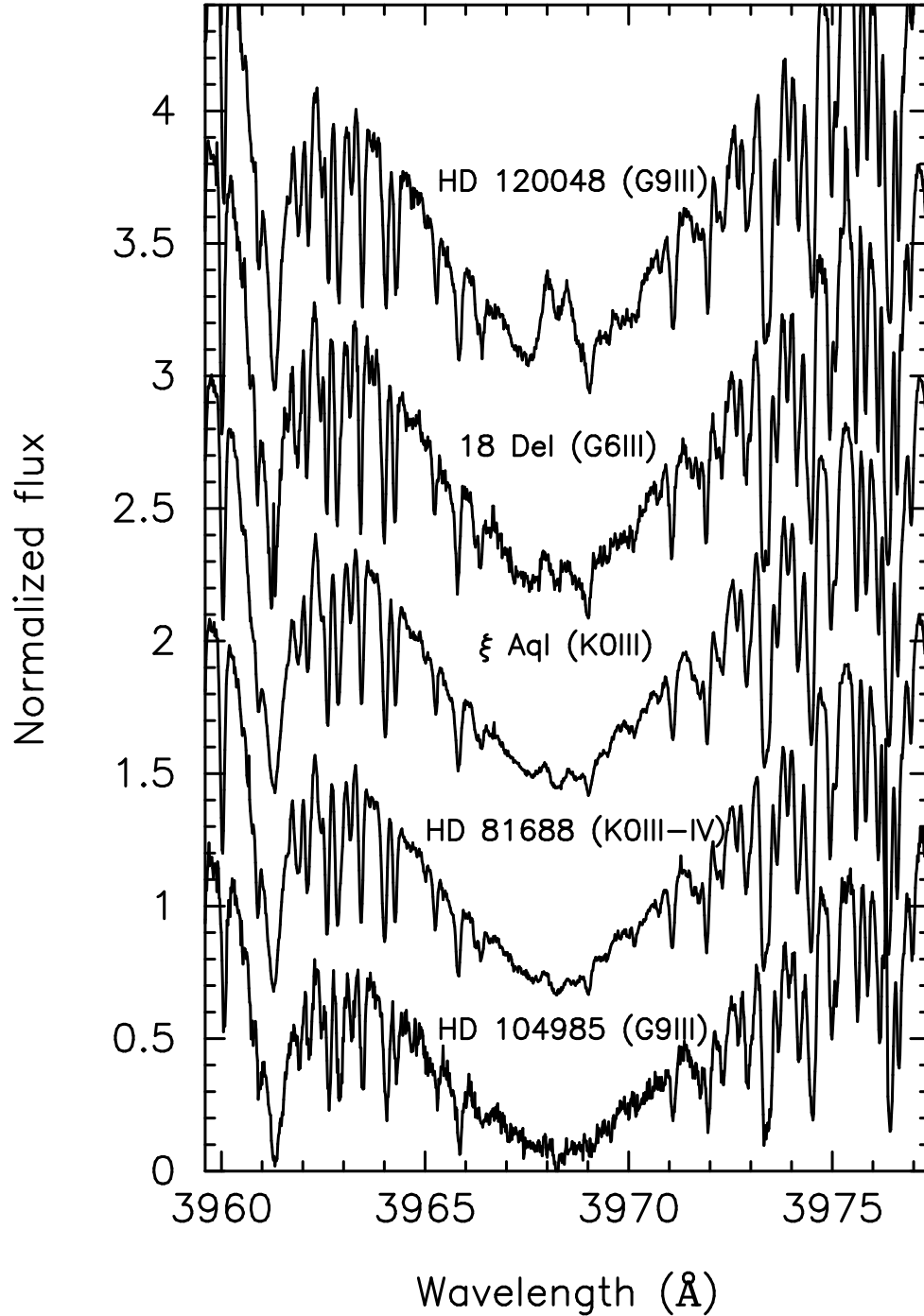


**Fig. 1.** Spectra in the region of Ca H lines.  $\xi$  Aql, HD 81688, and HD 104985 show no significant emissions in line cores. 18 Del shows slight core reversal but it is not significant compared to that in HD 120048, a chromospheric active star in our sample, which exhibits velocity scatter of about  $30 \text{ m s}^{-1}$  at most. A vertical offset of about 0.7 is added to each spectrum.

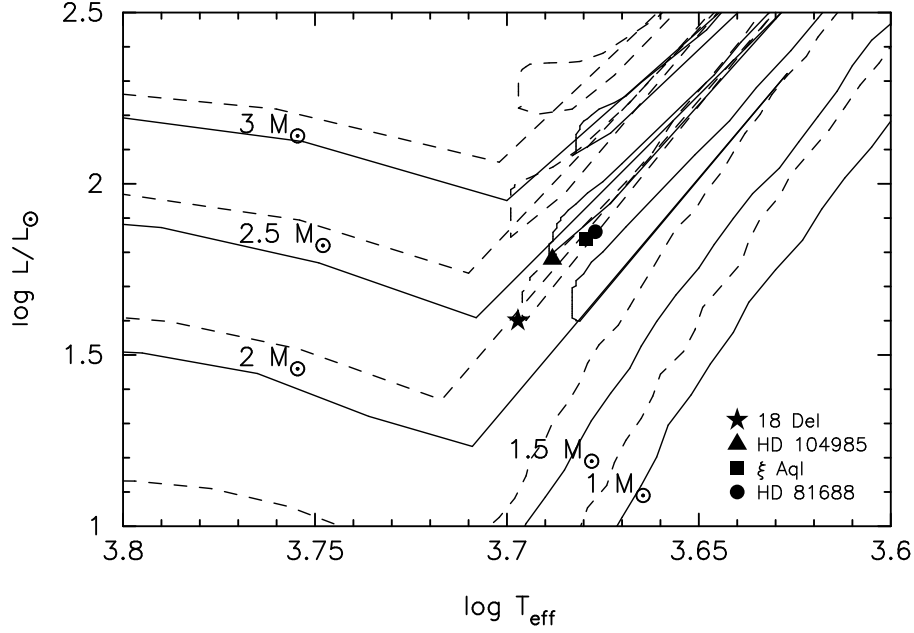


**Fig. 2.** HR diagram of the planet-harboring stars presented in this paper. Evolutionary tracks from Lejeune and Schaerer (2001) for stars with  $Z = 0.02$  (solar metallicity; solid lines) and  $Z = 0.008$  (dashed lines) of masses between 1 and  $3 M_{\odot}$  are also shown.

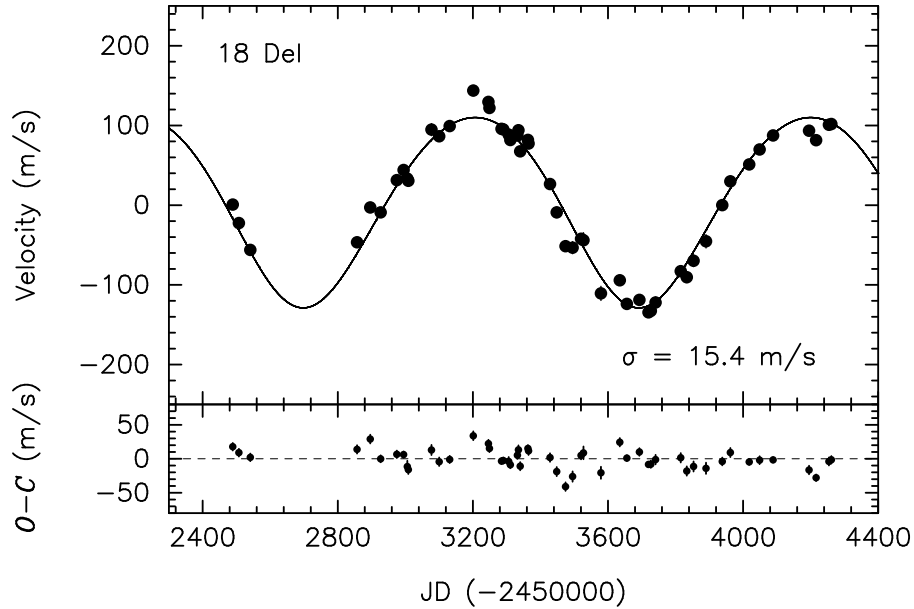


**Fig. 3.** *Top:* Observed radial velocities of 18 Del (dots). The Keplerian orbital fit is shown by the solid line. The period is 993 days, the velocity semi-amplitude is  $119 \text{ m s}^{-1}$ , and the eccentricity is 0.08. Adopting a stellar mass of  $2.3 M_{\odot}$ , we obtain the minimum mass for the companion of  $10.3 M_{\text{J}}$ , and semi-major axis of 2.6 AU. *Bottom:* Residuals to the Keplerian fit. The rms to the fit is  $15.4 \text{ m s}^{-1}$ .

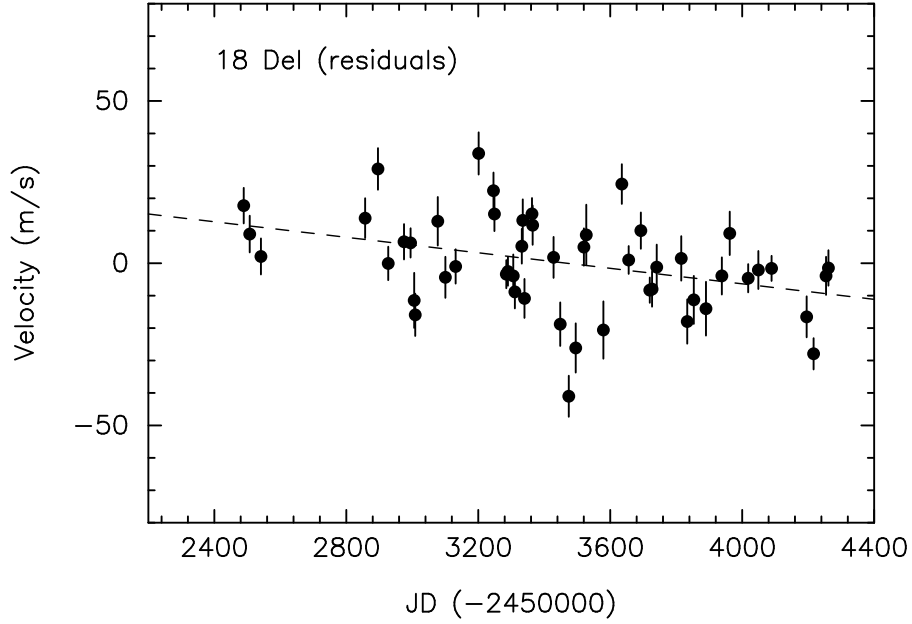


**Fig. 4.** Linear fit to the residuals to the Keplerian orbit for 18 Del. The dashed line shows the best-fit linear trend corresponding to  $-4.4 \text{ m s}^{-1} \text{ yr}^{-1}$ .

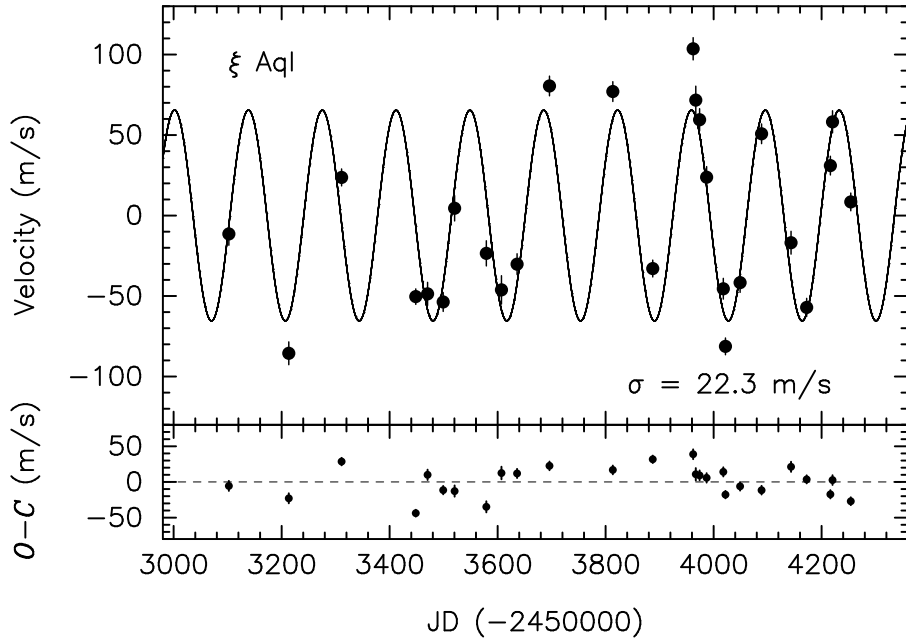


**Fig. 5.** *Top:* Observed radial velocities of  $\xi$  Aql (dots). The Keplerian orbital fit is shown by the solid line. The period is 136.8 days and the velocity semi-amplitude is  $65 \text{ m s}^{-1}$  (the eccentricity is fixed to zero). Adopting a stellar mass of  $2.2 M_{\odot}$ , we obtain the minimum mass for the companion of  $2.8 M_{\text{J}}$ , and semi-major axis of 0.68 AU. *Bottom:* Residuals to the Keplerian fit. The rms to the fit is  $22.3 \text{ m s}^{-1}$ .



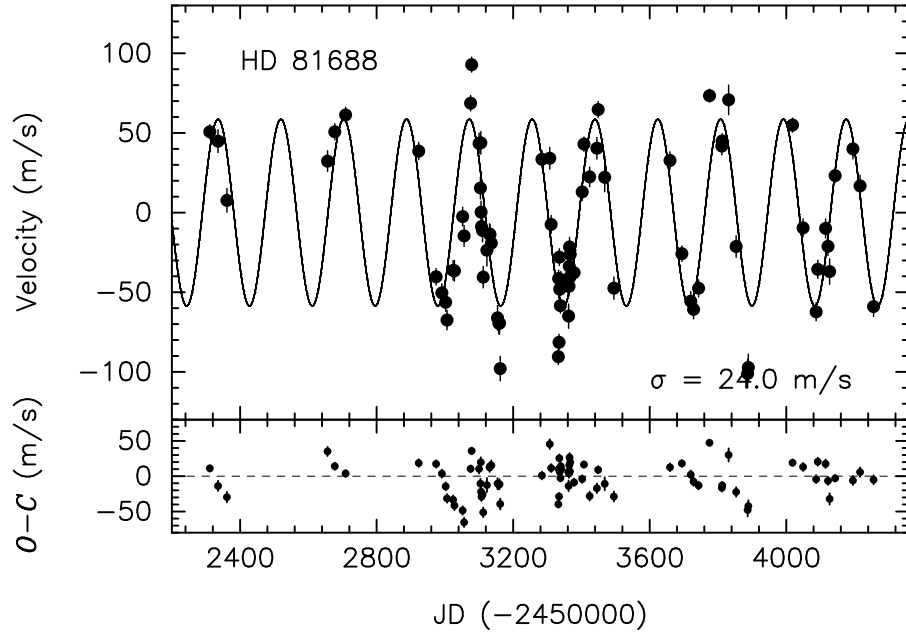


**Fig. 6.** *Top:* Observed radial velocities of HD 81688 (dots). The Keplerian orbital fit is shown by the solid line. The period is 184.0 days and the velocity semiamplitude is  $59 \text{ m s}^{-1}$  (the eccentricity is fixed to zero). Adopting a stellar mass of  $2.1 M_{\odot}$ , we obtain the minimum mass for the companion of  $2.7 M_{\text{J}}$ , and semimajor axis of 0.81 AU. *Bottom:* Residuals to the Keplerian fit. The rms to the fit is  $24.0 \text{ m s}^{-1}$ .

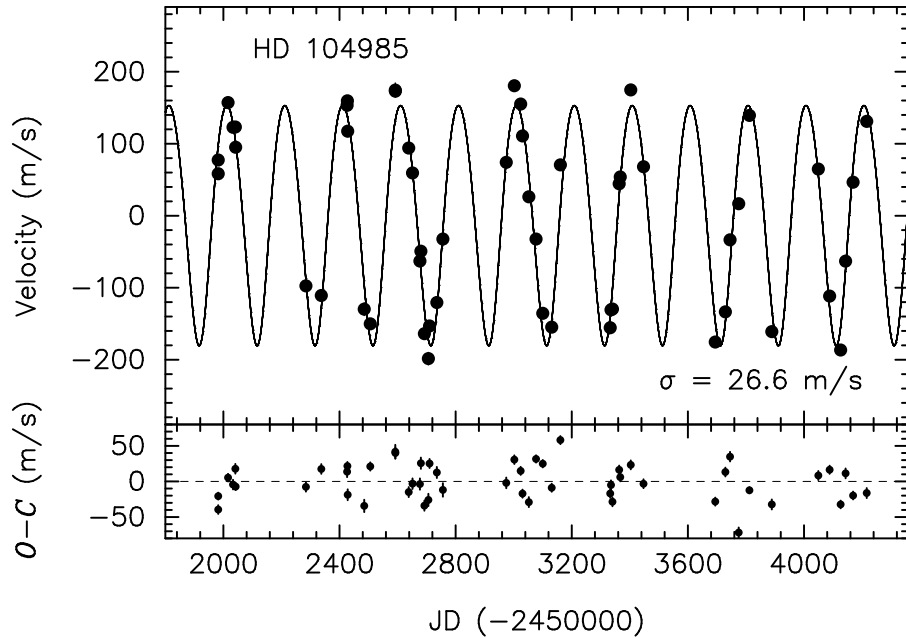


**Fig. 7.** *Top:* Observed radial velocities of HD 104985 (dots). The Keplerian orbital fit is shown by the solid line. The period is 199.51 days and the velocity semiamplitude is  $167 \text{ m s}^{-1}$ , and the eccentricity is 0.09. Adopting a stellar mass of  $2.3 M_{\odot}$ , we obtain the minimum mass for the companion of  $8.3 M_{\text{J}}$ , and semimajor axis of 0.95 AU. *Bottom:* Residuals to the Keplerian fit. The rms to the fit is  $26.6 \text{ m s}^{-1}$ .

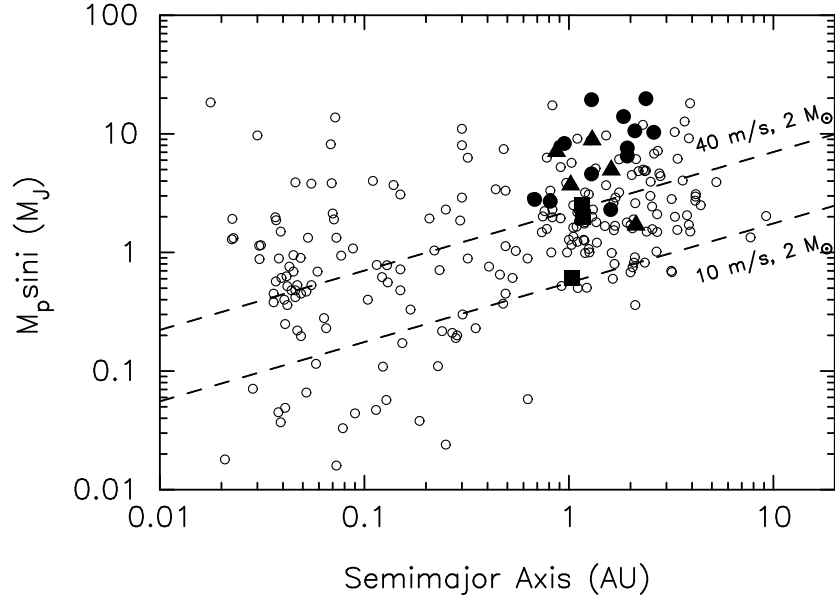


**Fig. 8.** Mass of extrasolar planets plotted against semimajor axis. Planets around low-mass ( $< 1.6M_{\odot}$ ) giants, intermediate-mass ( $1.6\text{--}1.9M_{\odot}$ ) subgiants, and clump giants ( $1.7\text{--}3.9M_{\odot}$ ), are plotted by filled triangles, filled squares, and filled circles, respectively. Planets around solar-type dwarfs are plotted by open circles.

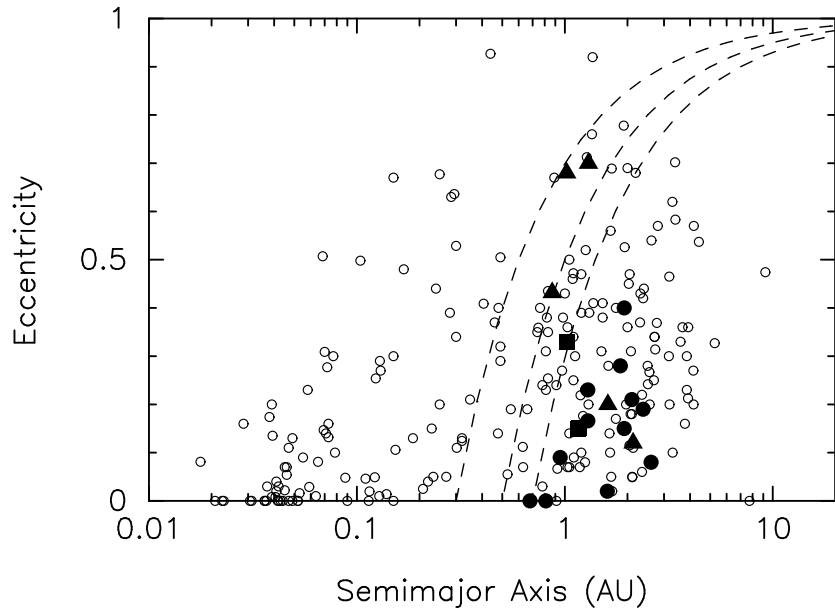


**Fig. 9.** Eccentricity of extrasolar planets plotted against semimajor axis. Planets around low-mass ( $< 1.6M_{\odot}$ ) giants, intermediate-mass ( $1.6\text{--}1.9M_{\odot}$ ) subgiants, and clump giants ( $1.7\text{--}3.9M_{\odot}$ ), are plotted by filled triangles, filled squares, and filled circles, respectively. Planets around solar-type dwarfs are plotted by open circles. Dashed lines express the periastron distance ( $q = a(1 - e)$ ) of 0.3, 0.5, 0.7 AU, respectively, from the left.

**Table 1.** Stellar parameters

Parameter	18 Del	$\xi$ Aql	HD 81688	Source/Method
Sp. Type	G6 III	K0 III	K0 III–IV	Hipparcos catalogue
$\pi$ (mas)	$13.68 \pm 0.70$	$15.96 \pm 1.01$	$11.33 \pm 0.84$	Hipparcos catalogue
$V$	5.51	4.71	5.40	Hipparcos catalogue
$B - V$	0.934	1.023	0.993	Hipparcos catalogue
$A_V$	0.04	0.10	0.10	Arenou et al's (1992) table
$M_V$	1.15	0.63	0.57	From $\pi$ , $V$ , and $A_V$
$B.C.$	-0.39	-0.48	-0.48	Kurucz (1993)'s theoretical calculation
$T_{\text{eff}}$ (K)	$4979 \pm 18$	$4780 \pm 30$	$4753 \pm 15$	Determined from Fe I and Fe II lines
$\log g$	$2.818 \pm 0.060$	$2.66 \pm 0.11$	$2.223 \pm 0.050$	Determined from Fe I and Fe II lines
$v_t$	$1.22 \pm 0.06$	$1.49 \pm 0.09$	$1.43 \pm 0.05$	Determined from Fe I and Fe II lines
[Fe/H]	$-0.052 \pm 0.023$	$-0.205 \pm 0.039$	$-0.359 \pm 0.020$	Determined from Fe I and Fe II lines
$L$ ( $L_{\odot}$ )	40	69	72	From $M_V$ and B.C.
$R$ ( $R_{\odot}$ )	8.5	12	13	From $T_{\text{eff}}$ and $L$
$M$ ( $M_{\odot}$ )	2.3	2.2	2.1	Lejeune & Schaerer's theoretical tracks
$v \sin i$ (km s $^{-1}$ )	-	2.0	1.2	de Medeiros & Mayor (1999)

Note – While the uncertainties of [Fe/H] are the rms errors ( $\equiv \sigma/\sqrt{N}$ ) relevant to the average over  $N$  lines, those given for  $T_{\text{eff}}$ ,  $\log g$ , and  $v_t$ , are nothing but the internal statistical errors (for a given data set of Fe I and Fe II line equivalent widths) evaluated by the procedure described in subsection 5.2 of Takeda et al. (2002). Actually, since these parameter values are sensitive to slight changes in the equivalent widths as well as to the adopted set of lines, realistic ambiguities may be by a factor of  $\sim 2$ – $3$  larger than these estimates from a conservative point of view (e.g., 50–100 K in  $T_{\text{eff}}$ , 0.1–0.2 dex in  $\log g$ ). It is normally difficult to precisely determine mass of clump giants and also set reliable error bars on it because stellar evolutionary tracks with various mass, metallicity and evolutionary status occupy similar position near the clump region on the HR diagram. Corresponding to the above uncertainties in the parameters of these stars assumed as  $\Delta T_{\text{eff}} \sim 100$  K,  $\Delta[\text{Fe}/\text{H}] \sim 0.1$  dex, and  $\Delta L/L_{\odot} \sim 5$ – $10\%$  (mostly due to Hipparcos parallax errors), errors for the mass and radius of these stars are estimated to be  $\Delta M \sim 0.2$ – $0.3 M_{\odot}$  and  $\Delta R/R_{\odot} \sim 5$ – $10\%$ . Moreover, we should keep in mind that the resulting mass value may appreciably depend on the chosen set of theoretical evolutionary tracks (e.g., the systematic difference as large as  $\sim 0.5 M_{\odot}$  for the case of metal-poor tracks between Lejeune & Schaerer (2001) and Girardi et al. (2000).; cf. footnote 3). Further comprehensive discussion of stellar parameters of late-G and early-K giants and their ambiguities, based on a larger number ( $\sim 320$ ) of sample stars, will be presented in a forthcoming paper (Takeda et al. in preparation).

**Table 2.** Radial Velocities of 18 Del

JD (-2450000)	Radial Velocity (m s <sup>-1</sup> )	Uncertainty (m s <sup>-1</sup> )
2489.1422	0.8	5.5
2507.1266	-22.4	5.7
2541.1260	-56.1	5.5
2857.1356	-46.5	6.1
2896.0403	-2.9	6.4
2927.0518	-9.1	5.2
2974.9012	31.4	5.5
2994.8978	44.1	4.5
3005.8960	33.2	8.5
3008.8873	30.6	6.5
3077.3450	94.8	7.5
3100.2914	86.4	6.3
3131.3138	99.2	5.3
3201.1162	143.8	6.5
3246.1069	129.6	5.6
3249.1072	122.0	5.3
3284.9244	95.7	4.3
3289.9548	95.1	4.4
3305.9224	88.6	6.6
3310.9473	81.8	5.1
3331.9186	87.3	5.4
3334.8762	94.0	6.5
3340.0094	67.5	6.0
3362.8767	81.9	4.9
3364.9064	77.3	6.1
3428.3705	26.5	6.3
3448.3432	-9.0	6.7
3474.3188	-51.5	6.3
3495.2623	-53.3	7.6
3520.2931	-42.2	5.8
3527.2996	-43.9	9.3
3579.1322	-110.6	8.8
3635.0984	-94.2	6.1
3655.9467	-123.8	4.3

**Table 2.** (Continued.)

JD (-2450000)	Radial Velocity (m s <sup>-1</sup> )	Uncertainty (m s <sup>-1</sup> )
3692.9010	-118.8	5.6
3719.9211	-134.4	3.9
3726.8798	-132.6	5.4
3740.8819	-122.1	7.0
3815.3434	-82.8	6.9
3833.3331	-90.4	6.8
3853.2909	-69.7	7.4
3890.2191	-45.3	8.3
3938.2715	0.1	5.7
3962.2112	29.9	6.7
4018.0439	51.1	4.4
4048.9950	69.9	5.9
4088.8993	87.5	3.9
4195.3185	93.4	6.3
4216.3152	81.6	4.8
4254.2312	100.9	5.9
4261.2661	101.9	5.5

**Table 3.** Orbital Parameters

Parameter	18 Del	$\xi$ Aql	HD 81688	HD 104985
$P$ (days)	993.3 $\pm$ 3.2	136.75 $\pm$ 0.25	184.02 $\pm$ 0.18	199.505 $\pm$ 0.085
$K_1$ (m s <sup>-1</sup> )	119.4 $\pm$ 1.3	65.4 $\pm$ 1.7	58.58 $\pm$ 0.97	166.8 $\pm$ 1.3
$e$	0.08 $\pm$ 0.01	0 (fixed)	0 (fixed)	0.090 $\pm$ 0.009
$\omega$ (deg)	166.1 $\pm$ 6.5	0 (fixed)	0 (fixed)	203.5 $\pm$ 5.7
$T_p$ (JD-2,450,000)	1672 $\pm$ 18	3001.7 $\pm$ 1.4	2335.4 $\pm$ 1.1	1927.5 $\pm$ 3.3
$a_1 \sin i$ (10 <sup>-3</sup> AU)	10.89 $\pm$ 0.11	0.824 $\pm$ 0.022	0.993 $\pm$ 0.016	3.053 $\pm$ 0.024
$f_1(m)$ (10 <sup>-7</sup> $M_\odot$ )	1.743 $\pm$ 0.054	0.0399 $\pm$ 0.0031	0.0385 $\pm$ 0.0019	0.953 $\pm$ 0.022
$m_2 \sin i$ ( $M_J$ )	10.3	2.8	2.7	8.3
$a$ (AU)	2.6	0.68	0.81	0.95
$N_{\text{obs}}$	51	26	81	52
rms (m s <sup>-1</sup> )	15.4	22.3	24.0	26.6
Reduced $\sqrt{\chi^2}$	2.5	3.8	3.9	4.1

**Table 4.** Radial Velocities of  $\xi$  Aql

JD (-2450000)	Radial Velocity (m s <sup>-1</sup> )	Uncertainty (m s <sup>-1</sup> )
3102.2929	-11.4	7.0
3213.1702	-85.6	7.1
3310.9914	23.7	5.3
3448.3230	-50.3	4.8
3470.3333	-48.7	7.2
3499.1952	-53.7	5.9
3520.3046	4.5	7.9
3579.0731	-23.5	7.8
3607.0846	-46.2	8.8
3636.0151	-30.2	6.5
3695.9542	80.5	6.1
3813.3486	77.0	6.2
3887.2842	-32.9	5.2
3962.0643	103.6	6.9
3967.0716	71.7	8.7
3974.0548	59.5	6.9
3987.0199	23.8	6.6
4018.0165	-45.5	6.5
4022.0373	-81.2	5.2
4048.9763	-41.7	6.1
4088.8857	50.7	6.1
4143.3757	-16.9	7.1
4172.3496	-57.1	5.6
4216.3038	31.0	5.8
4220.3112	58.2	6.9
4254.1264	8.5	5.5

**Table 5.** Radial Velocities of HD 81688

JD (-2450000)	Radial Velocity (m s <sup>-1</sup> )	Uncertainty (m s <sup>-1</sup> )
2311.1798	50.7	4.4
2335.2204	44.8	7.1
2361.2050	7.7	7.4
2656.0534	32.3	6.5
2677.2518	50.7	5.1
2709.1489	61.3	4.9
2923.3218	38.6	5.5
2974.2203	-40.3	5.2
2991.2026	-50.4	5.8
3002.1804	-56.3	5.7
3006.1215	-67.4	6.1
3024.0642	-36.3	6.2
3028.0500	-36.5	6.5
3052.0118	-2.5	5.9
3056.1429	-14.7	6.6
3075.0432	68.7	4.9
3078.2002	92.9	4.7
3100.0052	43.4	6.5
3104.1309	15.4	6.8
3105.1169	43.8	7.1
3106.0327	0.2	6.9
3107.1472	-8.8	6.1
3110.1677	-11.2	7.1
3112.0892	-40.5	6.7
3123.0991	-23.6	9.9
3131.0036	-13.5	6.5
3131.9477	-13.7	6.1
3136.0225	-19.2	6.9
3154.0323	-66.1	7.9
3157.9805	-69.5	6.7
3159.9783	-69.4	6.8
3162.0172	-97.9	7.7
3284.3176	33.5	5.5
3307.2533	34.1	6.8

Table 5. (Continued.)

JD (-2450000)	Radial Velocity (m s <sup>-1</sup> )	Uncertainty (m s <sup>-1</sup> )
3311.2119	-7.4	5.6
3332.3369	-90.5	4.9
3333.2075	-41.4	5.2
3334.2916	-81.4	5.0
3335.2195	-28.0	5.3
3336.2558	-48.1	4.8
3338.3409	-58.4	4.7
3339.3451	-42.1	5.2
3340.2926	-46.9	4.9
3361.3194	-45.9	6.1
3362.3774	-65.0	7.6
3363.3370	-46.3	6.1
3364.2794	-33.6	6.0
3365.2714	-21.5	6.0
3366.1669	-40.4	6.4
3367.1279	-26.2	6.1
3378.3533	-37.7	5.1
3402.2015	13.0	5.3
3407.2808	43.0	4.4
3424.0331	22.4	6.3
3445.1913	40.4	6.8
3449.0443	64.7	5.1
3468.1174	22.1	9.0
3495.0446	-47.4	7.0
3659.3268	32.7	5.5
3694.3233	-25.8	4.9
3720.3760	-55.6	6.1
3728.3348	-60.7	6.0
3743.2486	-47.5	5.4
3775.1171	73.4	4.0
3811.2229	41.7	5.4
3812.0871	44.9	4.7
3831.1137	70.8	9.3
3853.1140	-21.3	6.8
3886.9814	-101.0	9.0



**Table 5.** (Continued.)

JD (-2450000)	Radial Velocity (m s <sup>-1</sup> )	Uncertainty (m s <sup>-1</sup> )
3888.9868	-97.2	8.4
4018.3495	54.9	4.4
4049.2922	-9.6	5.7
4087.3587	-62.3	5.7
4092.2203	-35.6	5.7
4115.3330	-9.9	6.0
4122.2220	-21.2	5.7
4127.1958	-37.0	8.0
4143.2036	23.2	4.5
4195.1511	40.0	6.3
4216.0967	16.8	6.7
4255.9738	-59.0	6.3

**Table 6.** Radial Velocities of HD 104985

JD (-2450000)	Radial Velocity (m s <sup>-1</sup> )	Uncertainty (m s <sup>-1</sup> )
2284.3135	-97.5	6.6
2337.2114	-110.8	6.8
2425.9960	153.5	7.7
2426.9682	159.7	5.7
2427.9753	117.4	7.7
2484.9871	-129.7	8.7
2505.9601	-150.1	5.8
2592.2476	174.6	9.8
2592.3501	173.1	7.6
2638.3674	94.0	7.1
2651.3383	59.4	7.4
2677.1079	-63.0	7.9
2680.2379	-49.3	8.0
2692.2555	-163.8	7.1
2706.1590	-198.4	8.6
2710.1659	-153.1	6.3
2735.1287	-120.6	7.8
2756.1053	-32.4	9.5
2974.2742	74.2	7.5
3002.2274	180.6	6.1
3024.1295	155.2	5.7
3030.3033	110.8	5.6
3052.0835	26.3	7.0
3077.0500	-32.3	5.2
3100.0693	-135.6	5.2
3131.0540	-154.7	5.7
3160.9710	70.7	5.7
3332.3794	-155.5	6.2
3335.3282	-130.7	6.7
3340.3146	-129.6	6.2
3363.3593	44.4	6.0
3367.2023	53.9	5.9
3403.3051	174.8	6.3
3447.2055	68.0	6.3

**Table 6.** (Continued.)

JD (-2450000)	Radial Velocity (m s <sup>-1</sup> )	Uncertainty (m s <sup>-1</sup> )
3694.3459	-175.4	5.6
3729.3337	-133.6	6.3
3745.3168	-33.4	6.8
1982.1212	58.4	6.2
1982.1341	77.4	4.9
3775.2303	16.7	7.1
3812.1245	139.3	4.3
3889.0249	-161.0	7.0
2016.0945	157.3	5.4
2033.0394	122.9	6.8
2041.0056	123.2	6.8
2042.0112	95.1	5.0
4049.3406	64.8	6.4
4088.3821	-111.6	5.8
4126.3022	-186.5	5.4
4143.2217	-63.1	6.9
4169.0809	46.6	5.6
4216.1184	131.1	7.1

**Table 7.** Bisector Quantities

Bisector Quantities	18 Del	$\xi$ Aql	HD 81688	HD 104985
Bisector Velocity Span (BVS) (m s <sup>-1</sup> )	0.5±3.9	-3.9±5.2	6.4±4.8	10.7±4.9
Bisector Velocity Curve (BVC) (m s <sup>-1</sup> )	0.0±1.7	-1.2±1.8	4.0±3.3	-3.6±3.2
Bisector Velocity Displacement (BVD) (m s <sup>-1</sup> )	-205.8±10.1	-127.3±12.4	-139.37±14.3	-323.7±16.5

**Table 8.** Substellar Companions around Evolved Stars

HD		Sp. Type	$M_*$ ( $M_\odot$ )	$R_*$ ( $R_\odot$ )	$M_p \sin i$ ( $M_J$ )	$a$ (AU)	$e$	Ref.
Clump Giants								
	NGC 4349		3.9	–	19.8	2.38	0.19	1
13189		K2 II	2–7	–	8–20	1.5–2.2	0.28	2
28305	$\epsilon$ Tau	K0 III	2.7	13.7	7.6	1.93	0.15	3
107383	11 Com	G8 III	2.7	19	19.4	1.29	0.23	4
	NGC 2423		2.4	–	10.6	2.1	0.21	1
199665	18 Del	G6 III	2.3	8.5	10.3	2.6	0.08	5
104985		G9 III	2.3	11	8.3	0.95	0.09	5,6
17092		K0	2.3	10.1	4.6	1.29	0.166	7
188310	$\xi$ Aql	K0 III	2.2	12	2.8	0.68	0	5
81688		K0 III–IV	2.1	13	2.7	0.81	0	5
11977		G5 III	1.91	10.1	6.54	1.93	0.4	8
62509	$\beta$ Gem	K0 III	1.7	8.8	2.3	1.6	0.02	9
Subgiants								
210702		K1 IV	1.85	4.72	2.0	1.17	0.152	10
192699		G8 IV	1.68	4.25	2.5	1.16	0.149	10
175541		G8 IV	1.65	3.85	0.61	1.03	0.33	10
Low-mass K Giants								
222404	$\gamma$ Cep	K0 III	1.59	4.66	1.7	2.13	0.12	11
122430		K3 III	1.39	22.9	3.71	1.02	0.68	12
73108	4 UMa	K1 III	1.23	18.1	7.1	0.87	0.432	13
47536		K1 III	1.1	23.47	4.96	1.61	0.2	14
137759	$\iota$ Dra	K2 III	1.05	12.9	8.9	1.3	0.7	15

References.– (1) Lovis & Mayor (2007); (2) Hatzes et al. (2005); (3) Sato et al. (2007); (4) Liu et al. (2007); (5) This work; (6) Sato et al. (2003); (7) Niedzielski et al. (2007); (8) Setiawan et al. (2005); (9) Hatzes et al. (2006); (10) Johnson et al. (2007); (11) Hatzes et al. (2003); (12) Setiawan (2003); (13) Döllinger et al. (2007); (14) Setiawan et al. (2003); (15) Frink et al. (2002)